JOURNAL OF CATALYSIS 139, 664–678 (1993)

Fluorine-Mediated Acidity of Alumina-Pillared Fluorohectorite

JEAN-RÉMI BUTRUILLE,* LAURENT J. MICHOT,† ODILE BARRÈS,† AND THOMAS J. PINNAVAIA*,[1]

*Department of Chemistry and Center for Fundamental Materials Research, Michigan State University, East Lansing, Michigan 48824; and †Laboratoire Environnement et Minéralurgie, URA 235 du CNRS, BP 40, 54501 Vandoeuvre Cedex, France

Received July 13, 1992; revised September 28, 1992

Structural fluorine atoms in the 2 : 1 layered silicate framework of fluorohectorite have a profound effect on the acidity of alumina-pillared derivatives prepared by intecalation of Al_{13} polycations and subsequent calcination at elevated temperatures. The alumina-pillared clay formed by calcination at 350°C exhibits greatly enhanced catalytic activity for propylene alkylation of biphenyl, relative to nonfluorinated smectite hosts. However, calcination of the Al_{13} intercalate at 500°C results in a relatively inactive clay with greatly diminished NH_3 and pyridine chemisorption properties. The effect of the calcination process on the clay layer structure was carefully studied by ^{27}Al, ^{29}Si, and ^{19}F MAS-NMR and FTIR spectroscopic methods and by mass spectrometric analysis of volatile by-products. It was shown that between 30 and 500°C, specific lattice fluorine atoms adjacent to charged sites in the octahedral sheet of the layers are replaced by hydroxyl groups. At calcination temperatures below 350°C the Brønsted acidity of protonated hydroxyl groups in the layers is enhanced by the electron-withdrawing effect of near-neighbor fluorine atoms at neutral sites in the octahedral sheet. A mechanism for fluorine hydrolysis is proposed in which gallery water molecules, formed by the dehydroxylation of the alumina pillars, migrate to hexagonal oxygen cavities above the reactive fluorine positions. Between 350 and 500°C, a second process occurs that causes dehydroxylation of the layers, and this results in a sharp decrease in the acidity and catalytic activity of the pillared clay. The relationships between structure and reactivity suggest that the acid-catalytic activity of an alumina-pillared clay can be mediated by controlling the relative amounts of hydroxyl groups at charged octahedral sites and fluorine atoms at neutral octahedral sites in the host clay.

INTRODUCTION

Owing to growing environmental concerns over the disposal of depleted acid catalysts, there is interest in replacing tradition catalysts, such as aluminum chloride and hydrofluoric acid, with recyclable solid acids. In order to obtain materials competitive with the strongest homogeneous acid catalysts for organic isomerization, alkylation, and acetylation reactions, several strategies are being explored to improve the acidity of existing acidic compounds. Reactions of inorganic oxides with metal halides, for instance, have afforded strong acid materials (*1*). Fluorine, due to its strong electron–withdrawing properties, can improve the thermal stability and increase both the Lewis and the Brønsted acidity of an oxide when incorporated into the framework structure. It has been known for some time that the incorporation of fluorine in zeolites and related oxides enhances their acidity (*2, 3*). Fluorinated aluminas and silica–aluminas, in particular, can be stronger acids than concentrated sulfuric acid (*3*).

Much less work has been reported on the influence of fluorine substitution on the acidity of layered silicate clays. Fijal *et al.* have reported an improvement in catalytic properties of NH_4F-treated montmorillonite (*4*). However, it is difficult to introduce fluorine into a 2 : 1 smectite lattice without causing extensive destruction of the octahedral layer. It is much easier to introduce structural fluorine during the clay synthesis. In-

0021-9517/93 $5.00

deed, the synthesis of fluorohectorite has been known for some time (*5*). Suzuki *et al.* observed that fluorohectorite was much more active for the conversion of 2-propanol and ethanol than its nonfluorinated analogues (*6*). In the case of metal-oxide-pillared clays, Sakurai *et al.* reported an acidity enhancement for alumina-pillared fluortetrasilicic mica containing La^{3+} exchange ions (*7*).

We reported recently that alumina-pillared fluorohectorite was very active for the propene alkylation of liquid-phase biphenyl (*8*). This catalyst exhibited significant Brønsted acidity, which is unusual for alumina-pillared smectite clays. Only alumina-pillared beidellite was previously known to be a strong Brønsted acid (*9*). Most alumina-pillared clays exhibit strong Lewis acidity. We also have observed that the acid catalytic activity of alumina-pillared fluorohectorite clay is greatly reduced upon outgassing at temperatures above 350°C. That is, the presence of fluorine in the layer structure enhances the acidity of the alumina pillared clay at outgassing temperatures below 350°C, but at higher temperatures, the acidity is greatly diminished. In the present work we elucidate the structural factors which mediate the acidic properties of alumina-pillared fluorohectorite.

EXPERIMENTAL

Materials

A high charge density synthetic Li^+-fluorohectorite with a cation exchange capacity of 150 meq/100 g was used for pillared clay synthesis. The pillaring agent was the Keggin-like ion $[Al_{13}O_4(OH)_{24}(H_2O)_{12}]^{7+}$ generated by base hydrolysis of an aluminum chloride solution at an OH/Al molar ratio of 2.4. Aqueous suspensions of clay (1 wt%) were added slowly at room temperature to the vigorously stirred pillaring solution containing aluminum in large excess (15 mmol Al/meq clay). The reaction mixture was aged 12 h at room temperature, and the flocculated clay was then washed free of chloride ion (as observed by $AgNO_3$ test) by repeatingly placing the clay in suspension in deionized water and then centrifuging. The final products were air-dried on glass plates and then calcined in air 12 h at the desired temperature.

A low charge density synthetic Li^+-fluorohectorite, Laponite B, with a cation exchange capacity of 73 meq/100 g, was obtained from Laporte. This material was used as received for confirmatory ^{19}F MAS-NMR measurements.

Clay Characterization

Cationic exchange capacities (CEC) for Li^+-fluorohectorite and Li^+-Laponite were measured according to the procedure described by Busenberg and Clemency (*10*). The clay was ammonium exchanged with ammonium acetate, air-dried, and then resuspended in water. The amount of ammonia liberated under strong basic treatment was measured with an ammonia-specific electrode.

Li and Mg analysis were carried out by the University of Illinois Elemental Analysis Laboratory. X-ray diffraction patterns (CuK_α) of oriented films were obtained with a Rigaku X-ray diffractometer equipped with a rotating anode. Continuous flow N_2 adsorption–desorption isotherms at 77 K were obtained on a Coulter Omnisorb 360 CX sorptometer. All samples were outgassed at 150°C for 12 h under 10^{-4} Torr.

Temperature-programmed ammonia desorption (TPD) curves were obtained for 200-mg samples of pillared fluorohectorite. The catalysts were outgassed at 350°C prior to NH_3 adsorption at 100°C. The catalysts were then heated at 10°C/min and the molecules desorbed were detected by a thermal conductivity detector. The FTIR spectrum for chemisorbed pyridine was obtained on an IBM IR44 spectrometer. Self-supported pellets of the catalyst were outgassed 1 h at 300°C prior to pyridine adsorption at 150°C. A minimum outgassing time of 16 h at 150°C was necessary to remove most of the physically adsorbed pyridine. Chemisorbed pyridine was then further desorbed by evacua-

tion at 250 and 350°C for 45 min. All spectra were recorded at 150°C.

^{29}Si, ^{27}Al, and ^{19}F MAS-NMR spectra were obtained on a Varian VXR 400 spectrometer. A Bruker probe was used to spin the samples at 4 kHz for ^{29}Si and ^{27}Al MAS-NMR. A delay time of 480 s allowed full relaxation of the Si nucleus. The chemical shifts for ^{29}Si and ^{27}Al, respectively, are reported relative to tetramethylsilane and $[Al(H_2O)_6]^{3+}$. ^{19}F MAS-NMR spectra were obtained using a Doty probe with 35-s delay time and a spinning rate of 9 kHz. The ^{19}F chemical shifts are relative to hexafluorobenzene (δ ($CFCl_3$) = 164.9 ppm relative to hexafluorobenzene).

The IR-MS results were obtained on a Bruker IFS 88 Fourier transform spectrometer coupled to a Balzers QMG 420 C quadrupole mass spectrometer. This instrument is capable of discriminating masses between 0 and 200. KBr pellets of the solid sample (2.5 wt%) were mounted in a special cell where both the temperature (−20 to 1000°C) and pressure (10^{-7} Torr to atmospheric pressure) could be controlled. The cell windows were polished KBr.

Catalysis

The alkylation of biphenyl by propene was carried out in a 300-ml batch reactor (Parr Instruments No. 4561). Propene was CP grade (Matheson Company), and biphenyl was practical grade (Baker Company). Biphenyl (30 g, 0.194 mole) and 0.20 g of catalyst were heated to 90°C. The system was purged with propene under stirring until the temperature reached 150°C. Temperature and propene pressure were then carefully increased until they reached the final conditions of 250°C and 9.5 atm. After 20 h reaction time, the reaction mixture was cooled to room temperature and the products were dissolved in 300 ml toluene. The catalyst was filtered off, and the filtrate was analyzed by gas chromatography. The degree of alkylation was determined by GC–MS.

RESULTS

Synthesis

The reaction of Li^+-fluorohectorite (CEC = 150 meq/100 g) with excess $[Al_{13}O_4(OH)_{24}(H_2O)_{12}]^{7+}$ formed by base hydrolysis of $AlCl_3$ (OH^-/Al = 2.4, 15 mmol Al/meq clay) affords an alumina-pillared fluorohectorite (henceforth abbreviated APF) with a basal spacing of 19.2 Å (gallery height = 9.6 Å) under air-dried conditions.

As shown by the data in Table 1, the N_2 BET surface area of the pillared derivative depends greatly on the calcination temperature. An air-dried APF sample, when outgassed at 150°C, exhibits an optimum surface area of 348 m^2/g. Calcination at 250 and 350°C results in a loss of up to one-third the initial surface area, but calcination at 500°C restores the surface area to nearly its original value (325 m^2/g). The surface areas derived from t-plots of the nitrogen adsorption data parallel the BET values. Also, the t-plots reveal that the pillared product remains highly microporous at calcination temperatures up to 500°C. The microporous surface areas in Table 1 indicate that at least two-thirds of the total N_2 surface area falls in the microporous region (≤20 Å diameter), regardless of the calcination temperature. The mesoporous surface areas, as determined from the t-plots, fall in the range 45–69 m^2/g. The mesopore surface areas are not correlated with the calcination temperature. This is the behavior expected based on mesoporosity originating from particle texture and interparticle contacts. However, the dependence of microporosity on temperature suggests that important structural changes occur in the pillar and/or the layers with increasing calcination temperature. Also, earlier ^{29}Si MAS-NMR work has shown that some rearrangement of the layers most likely occurs upon calcination of APF (*11*).

Since the basal spacing of APFs decreases from 19.2 Å at 25°C to 18.2 Å at 350°C (cf. Table 1), a contraction in gallery height could contribute to the decrease in surface area over this temperature range. However,

TABLE 1

Basal Spacing and Surface Area Analysis of Alumina-Pillared Fluorohectorite Calcined at Various Temperatures[a]

Sample	Calcination temperature (°C)	Basal spacing d_{001} (Å)	S_{BET} (m^2/g)	$S_{t\text{-plot}}$	S_{micro}	$S_{meso\text{-}macro}$
APF	Uncalcined	19.2	348	380	319	45
APF-250	250	18.7	301	334	248	66
APF-350	350	18.2	214	234	175	56
APF-500	500	17.9	325	340	273	69

[a] The outgassing of the samples was carried out under vacuum (10^{-4} Torr) at 150°C for a period of 12 h.

the effects of gallery height contraction on surface area most likely are small, because calcination at 500°C causes the surface area to increase, despite an additional 0.3 Å decrease in gallery height. Thus, the temperature dependence of the surface area and microporosity of APF is attributable to changes in the constitution or distribution of the pillars, not on the reduction of gallery height.

Catalytic Activity and Acidity

We previously have shown (*8*) that alumina-pillared smectite clays are effective shape selective catalysts for the propene alkylation of liquid-phase biphenyl at 250°C. In general, alkylation activity is retained even when the clay is calcined at 500°C. Under the reaction conditions described in Table 2, alumina-pillared montmorillonite calcined at either 350 or 500°C converts about 60% of liquid-phase biphenyl to mainly mono- and dialkylated products. However, APF is an exception. As shown by the activity data in Table 2, catalysts, APF-250 and -350, which were prepared by calcination at 250 and 350°C, respectively, exhibit conversions that are dramatically higher than the material calcined at 500°C (i.e., APF-500). For APF-350, which is

TABLE 2

Biphenyl Conversions and Product Distributions Achieved with Calcined Alumina-Pillared Fluorohectorites and Alumina-Pillared Montmorillonite[a]

Catalyst	Alumina-pillared F-hectorites			Alumina-pillared montmorillonite[b]
	APF-250	APF-350	APF-500	
Biphenyl conversion (%)	84	98	23	64
Product distribution (%)				
Monoalkyl isomers	44	11	85	63
Dialkyl isomers	41	33	14	30
Trialkyl isomers	13	38	1	7
Tetraalkyl isomers	2	17	0	0

[a] The reaction conditions were are follows: 30 g biphenyl 0.2 g of a 100–200 mesh fraction of catalyst, 140 psi propylene, 250°C, 20 h reaction time.

[b] The alumina-pillared montmorillonite (Wyoming) was calcined at 350°C before use. Similar conversions and product distributions were obtained for the same catalyst after calcination at 500°C.

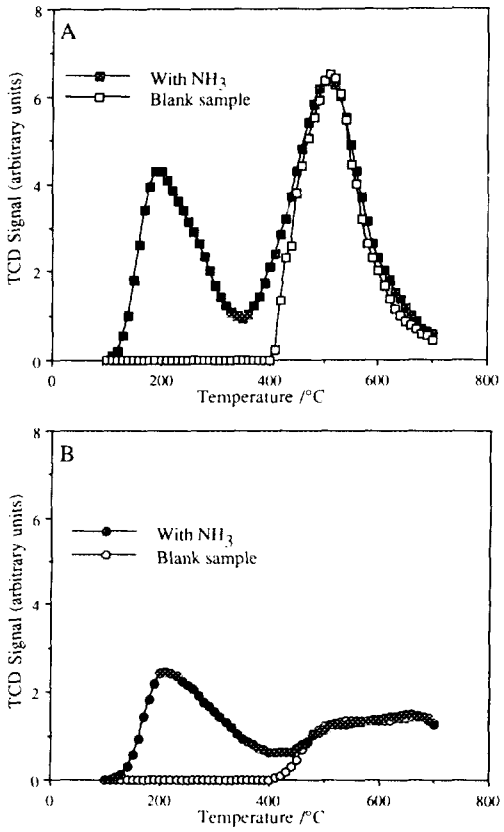

FIG. 1. Ammonia TPD experiments of alumina-pillared fluorohectorite calcined at (A) 350°C (APF-350) and (B) 500°C (APF-500), solid symbols, and blank experiments (without ammonia adsorption) on the same samples, open symbols.

somewhat more active than APF-250, almost all the biphenyl was alkylated, mainly to di- and trialkyl isomers. Thus, APF-350 is substantially more active as an alkylation catalyst than a typical nonfluorinated pillared smectite clay. In fact, APF-350 is even more active than the strong Brønsted-acid catalyst dealuminated mordenite, which affords only ~60% biphenyl conversion under analogous reaction conditions. Although APF-350 is an exceptionally active alkylation catalyst, calcination of the clay at 500°C dramatically reduces the alkylation activity. As shown by the data in Table 2 for APF-500, only 23% biphenyl conversion is achieved with this material, as compared with 98% conversion with APF-350.

In order to better elucidate the differences in alkylation activity for APF-350 and -500, we have examined the sorption of ammonia and pyridine on these materials. Figure 1 illustrates the results of the ammonia TPD experiments. Included in the figure are curves for blank samples of the two clays in the absence of adsorbed ammonia. The maxima centered near 500°C for the blank samples are attributable to volatile products resulting from structural rearrangement. TGA curves shown in Fig. 2 for the pristine clays verify the loss of mass above 350°. Returning to the TPD curves in Fig. 1, we see that APF-350 and -500 both exhibit NH_3 desorption peaks centered near 200°C. The

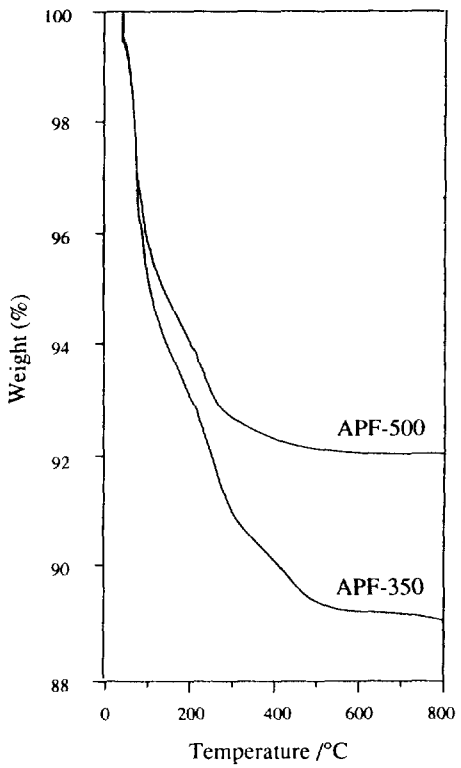

FIG. 2. Thermogravimetric analysis of alumina-pillared fluorohectorite calcined at 350°C (APF-350) and alumina-pillared fluorohectorite calcined at 500°C (APF-500).

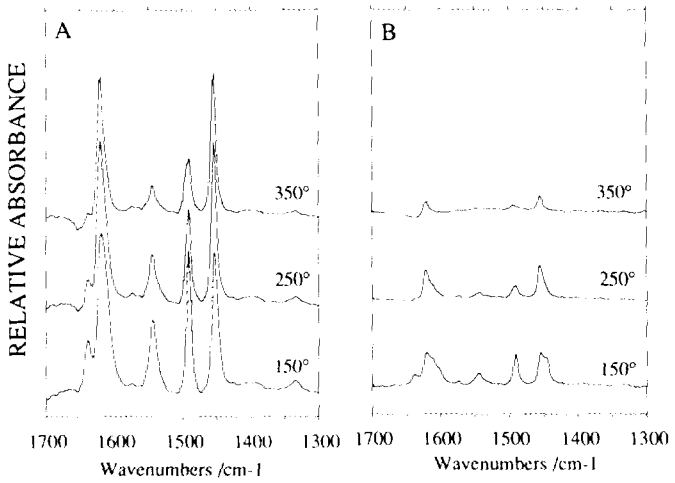

FIG. 3. Infrared spectra of pyridine adsorbed on alumina-pillared fluorohectorite calcined at (A) 350°C (APF-350), and (B) 500°C (APF-500). Pyridine-adsorbed sample was evacuated at 150, 250, and 350°C.

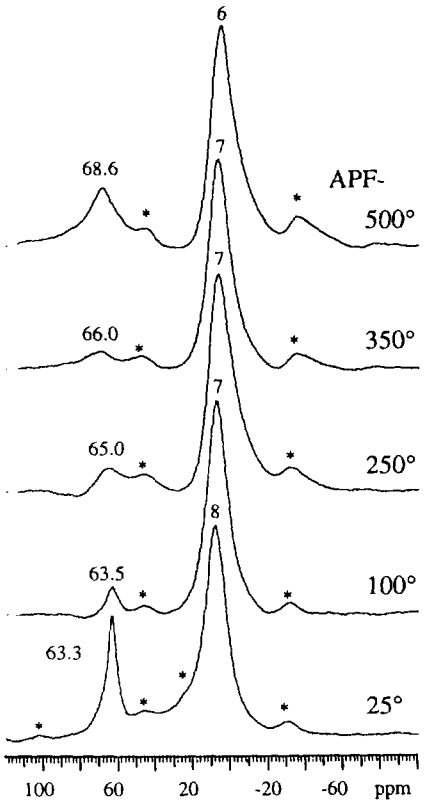

FIG. 4. ^{27}Al MAS-NMR spectra of alumina-pillared fluorohectorites that have been dried in air at the following temperatures: 25, 100, 250, 350, and 500°C. Chemical shifts are relative to $[Al(H_2O)_6]Cl_3$.

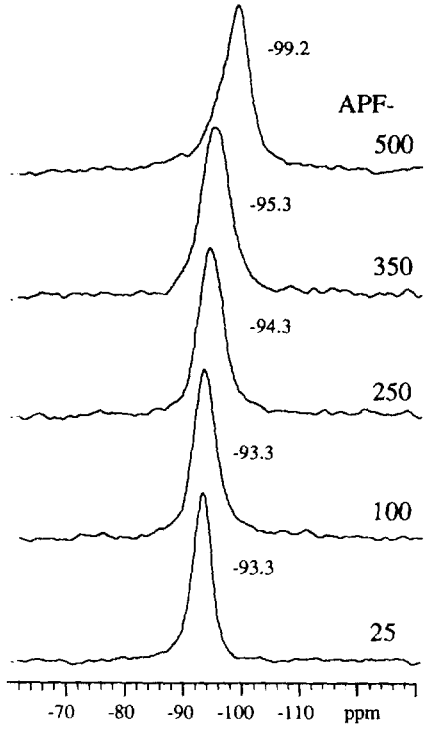

FIG. 5. ^{29}Si MAS-NMR spectra of alumina-pillared fluorohectorites that have been dried in air at the following temperatures: 25, 100, 250, 350, and 500°C. Chemical shifts are relative to TMS.

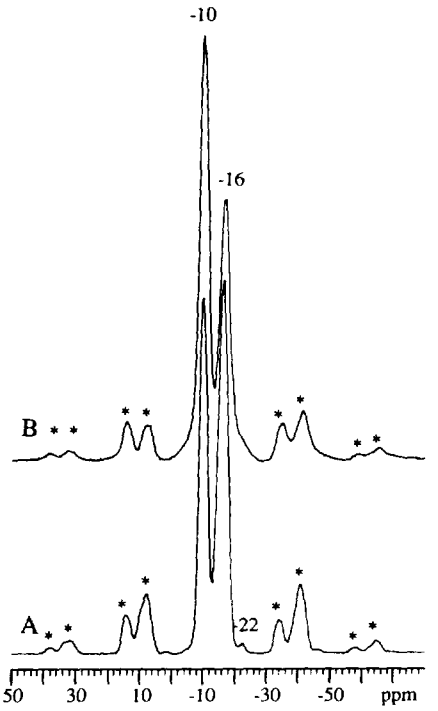

FIG. 6. ^{19}F MAS-NMR spectra of: (A) Li^+-fluorohectorite, (B) Li^+-Laponite B (calcined). Chemical shifts are relative to C_6F_6.

asymmetry in the peaks suggests a distribution of acid strengths. Integration of the TPD curves over the temperature range 100–350°C reveals that the amount of NH_3 chemically bound to APF-350 is approximately twice that for APF-500. Thus, the ammonia TPD results verify the presence of a substantially larger number of acid sites for APF-350.

The thermal desorption of chemisorbed pyridine, as monitored by FTIR, is shown in Fig. 3. These results also reveal significant differences in the acidity of APF-350 and APF-500. For APF-350, both Brønsted and Lewis acid sites are present even after desorption at 350°C, as evidenced by the pyridine ring stretching frequencies at 1545 and 1450 cm^{-1}, respectively. In contrast, the fewer acid sites present on APF-500 are mostly of the Lewis type. Using the molar extinction coefficients provided by Datka (*12*) for chemisorbed pyridine, we estimate the total number of acid sites present on APF-350 at 150°C to be 24 mmol/100 g with the Lewis-to-Brønsted ratio being 1.4. For APF-500 the total amount of bound pyridine at 350°C is 1.5 mmol/100 g with no Brønsted sites present. Thus, the acid sites on APF-350 are both more numerous and stronger than those present in APF-500.

MAS-NMR Spectroscopy

The thermochemical alterations indicated by the differences in NH_3 and pyridine sorption for APF-350 and -500, as well as by the TGA curves (cf. Fig. 2), were further studied by ^{27}Al, ^{29}Si and ^{19}F MAS-NMR. As shown by the ^{27}Al spectra in Fig. 4, a reso-

TABLE 3

Octahedral Metal Ion Compositions Based on an $O_{20}F_4$ Unit Cell for Two Fluorohectorites and Cation Exchange Capacities

	Fluorohectorite	Laponite B
Ratio of −10/−16 ppm ^{19}F intensities	0.78	1.85
Composition calculated from ^{19}F NMR	$Mg_{4.88}Li_{1.12}$	$Mg_{5.30}Li_{0.70}$
Cation exchange capacity (meq/100 g)	150	73
Composition calculated from CEC	$Mg_{4.82}Li_{1.18}$	$Mg_{5.42}Li_{0.58}$
Mg/Li mole ratio	1.47	6.57
Composition calculated from elemental analysis	$Mg_{4.46}Li_{1.54}$	$Mg_{5.58}Li_{0.42}$

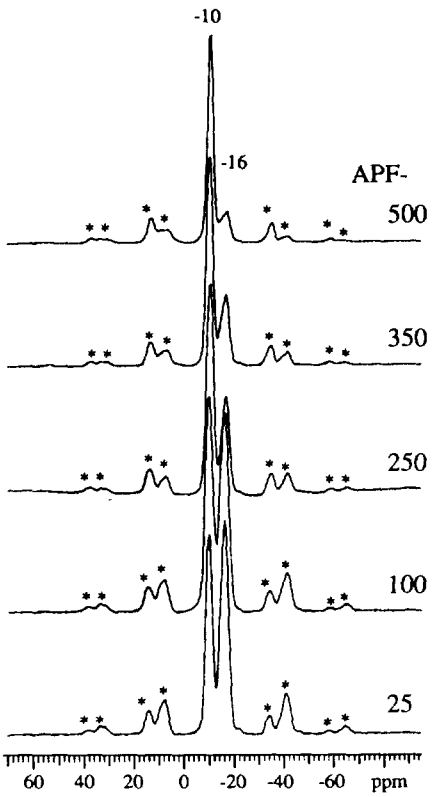

FIG. 7. ^{19}F MAS-NMR spectra of alumina pillared fluorohectorites that have been dried in air at the following temperatures: 25, 100, 250, 350, and 500°C. Chemical shifts are relative to C_6F_6.

nance characteristic of tetrahedral aluminum is observed for air-dried APF before calcination. This resonance, together with the peak for octahedral aluminum near 8 ppm, is characteristic of the intercalated Al_{13} oligomer (*13*). Upon calcination of the sample up to 350°C, the tetrahedral signal gradually decreases in intensity and broadens. After calcination at 500°C the tetrahedral signal increases in intensity and shifts downfield to 69 ppm, while the octahedral signal shifts slightly upfield to 6 ppm. A shift in the ^{29}Si resonance of APF also is observed upon calcination. As shown in Fig. 5, the silicon chemical shift moves from −92 ppm for air-dried APF to −99 ppm for APF-500. The appearance of a high-field ^{29}Si resonance has been observed previously for calcined alumina-pillared derivatives of fluorohectorite (*11*) and hectorite (*14*). These changes in the ^{27}Al and ^{29}Si chemical shifts indicate that important structural changes occur upon calcination of APF, especially when the calcination temperature is near 500°C.

The ^{19}F MAS-NMR spectrum of a natural fluorine-containing hectorite has been recently reported by Huve *et al.* (*15*) to exhibit two resonances. We also observe two nonequivalent environments for fluorohectorite. To assist in the ^{19}F chemical shift assignments, we have included in this study the spectrum of Laponite B, a low charge density fluorohectorite. Figure 6 compares the ^{19}F spectrum for the high charge density Li^+-fluorohectorite used in the pillaring experiments (CEC = 150 meq/100g) with the spectrum for low charge density Laponite (CEC = 73 meq/100g). The two clays exhibit two ^{19}F signals near −10 and −16 ppm. The low-field/high-field peak intensity ratio, as determined by deconvolution of overlapping Lorentzian and Gaussian lineshapes, were dependent on the layer charge densities of the two clays. These ratios are presented in Table 3, together with the CEC and elemental analyses for these clays.

The changes which occur in the ^{19}F MAS-NMR spectra for APF as a function of calcination temperature are presented in Fig. 7. The pillared clay dried at 25°C exhibits the same two ^{19}F resonances as the Li^+-exchanged form. However, upon calcination of the pillared clay over the temperature range 100–500°C, the intensity of the high-field resonance decreases eventually to ~15% of its initial value. This loss of structural fluorine over the temperature range 350–500°C is correlated with the decrease in acid catalytic activity.

FTIR Spectroscopy

An effort was made to examine the loss of structural fluorine from APF by FTIR spectroscopy. The temperature-dependent vibrational spectra for Li^+-fluorohectorite in Fig. 8 are compared with those for APF in Fig. 9. Li^+-fluorohectorite outgassed at

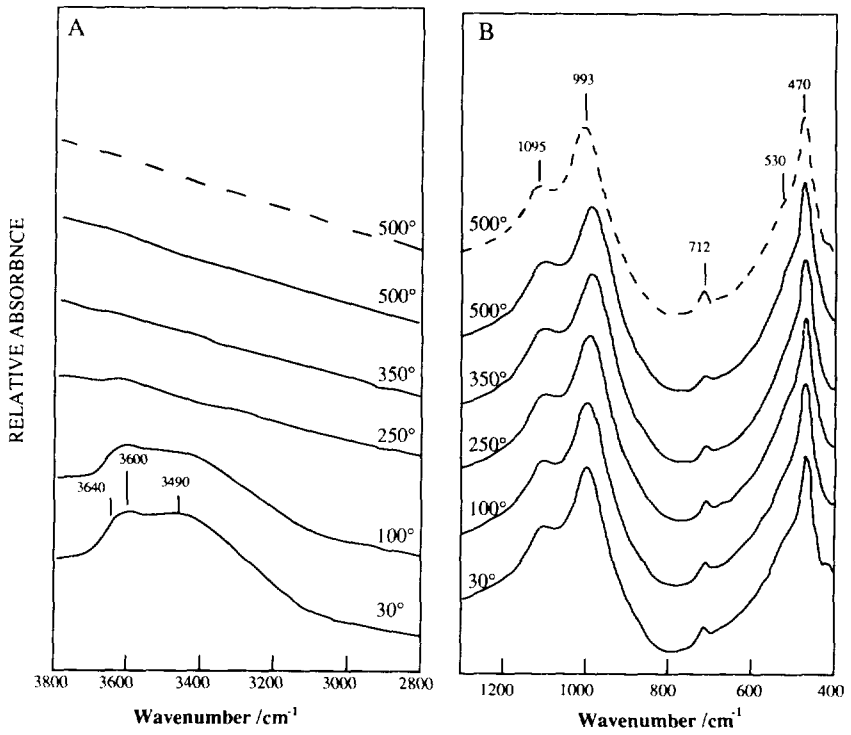

FIG. 8. Infrared spectra for Li^+ fluorohectorite obtained at different temperatures: (A) for the spectral range 3800–2800 cm^{-1}; (B) for the spectral range 1300–400 cm^{-1}. All spectra were recorded uncer vacuum at the temperature indicated, except for the dashed spectrum, for which the sample was heated to 500°C and subsequently cooled to room temperature to record the spectrum.

30°C exhibits stretching frequencies characteristic of coordinated water (ν_s = 3600, ν_a = 3640 cm^{-1}) and water of hydration (3490 cm^{-1}) (*16*). Several bands characteristic of the layered framework structure appear in the region 1300–400 cm^{-1}, including symmetric and asymmetric SiOSi vibrations at 1095 and 993 cm^{-1}, a shoulder at ~530 cm^{-1} corresponding to MgO stretching, and an SiO bending band at 470 cm^{-1} (*17*). The relatively weak band at 712 cm^{-1} is assigned to a metal–fluorine stretching vibration (*18*). As the outgassing temperature is increased to 250°C and beyond, the galleries become dehydrated and the vibrations due to OH-stretching bonds are virtually eliminated. Little or no change occurs, however, in the vibrations of the layered framework upon outgassing Li^+-fluorohectorite at temperatures as high as 500°C.

Owing to the presence of the intercalated Al_{13} oligomer, the FTIR spectral features of APF differ significantly from those of the Li^+-exchanged precursor. As shown by a comparison of Figs. 8A and 9A, the OH-stretching region of APF-30 is broader than that observed for the corresponding Li^+ derivative. Also, a new band is present at 756 cm^{-1}, which we tentatively assign to an Al–O stretching vibration of the Al_{13} oligomer. Upon thermal dehydration of APF, the absorbance in the hydroxyl group region decreases, but an OH vibration at 3680 cm^{-1} persists even after outgassing at 500°C (see spectrum APF-500 in Fig. 9A). Also, significant changes occur in the framework vibrations of APF, especially above 350°C. The SiOSi band at 1001 cm^{-1} in APF-30 shifts progressively to 1012 cm^{-1} in APF-500. Also, a comparison of the spectra for

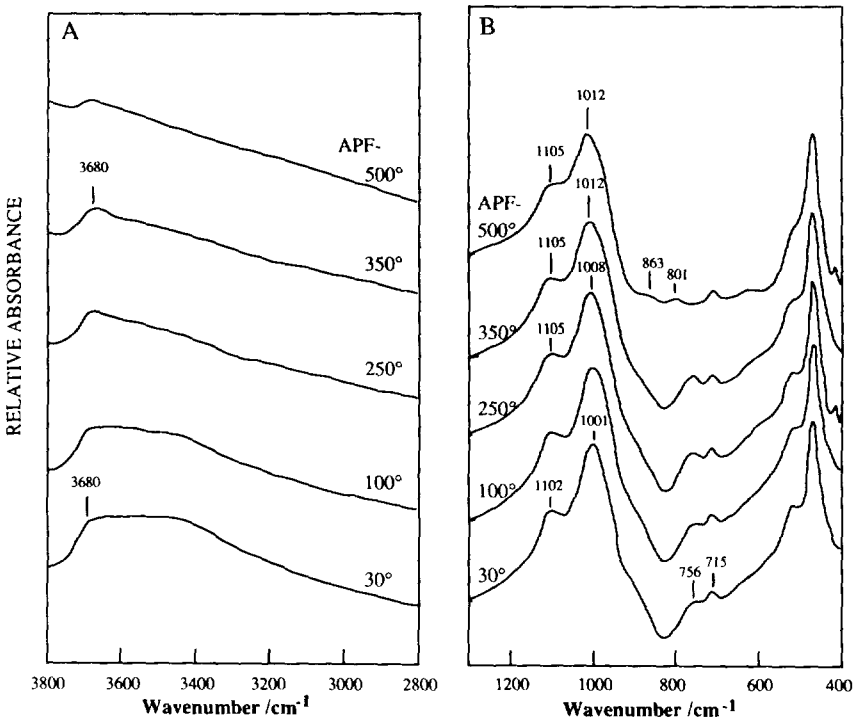

FIG. 9. Infrared spectra for alumina pillared fluorohectorite obtained at different temperatures: (A) in the range 3800–2800 cm^{-1}; (B) in the range 1300–400 cm^{-1}. All spectra were recorded under vacuum at 30°C.

APF-350 and APF-500 in Fig. 9B indicates the replacement of the 756 cm^{-1} band of the oligomer by two new bands at 863 and 801 cm^{-1}. These latter changes suggest a possible modification of the pillar, even though the basal spacings for APF-350 and APF-500 are similar ($d_{001} \approx 18$ Å). However, the FTIR data do not provide a direct indication for the loss of fluorine from the layer framework, as the metal–fluorine vibration at 715 cm^{-1} is retained throughout the entire temperature range investigated.

Mass Spectrometry

Our mass spectral studies suggest that at least some of the fluorine lost from the framework structure of APF can be detected in the gas phase. Figure 10A presents the mass spectra for the volatiles eliminated from Li^+-fluorohectorite when heated at 250°C. The spectra for this unpillared precursors show the elimination of water and trace amounts of surface contaminants such as CO_2. Analogous mass spectra for APF are given in Fig. 10B. In contrast to Li^+-fluorohectorite, the alumina-pillared product eliminates volatiles with mass numbers of 19 and 20, corresponding to F and HF, respectively. The evolution of the intensity of the mass 18, 19, and 20 peaks with temperature is presented in Fig. 11. The intensities of mass 19 and 20 increase most rapidly between 200–350°C.

DISCUSSION

Alumina-pillared fluorohectorite calcined at 350°C (i.e., APF-350) is an exceptionally active pillared clay catalyst. The acidity of this material is reflected in the propylene alkylation of liquid-phase biphenyl (cf. Table 2) the adsorption of ammonia (cf. Fig. 1), and in the chemisorption of pyridine through

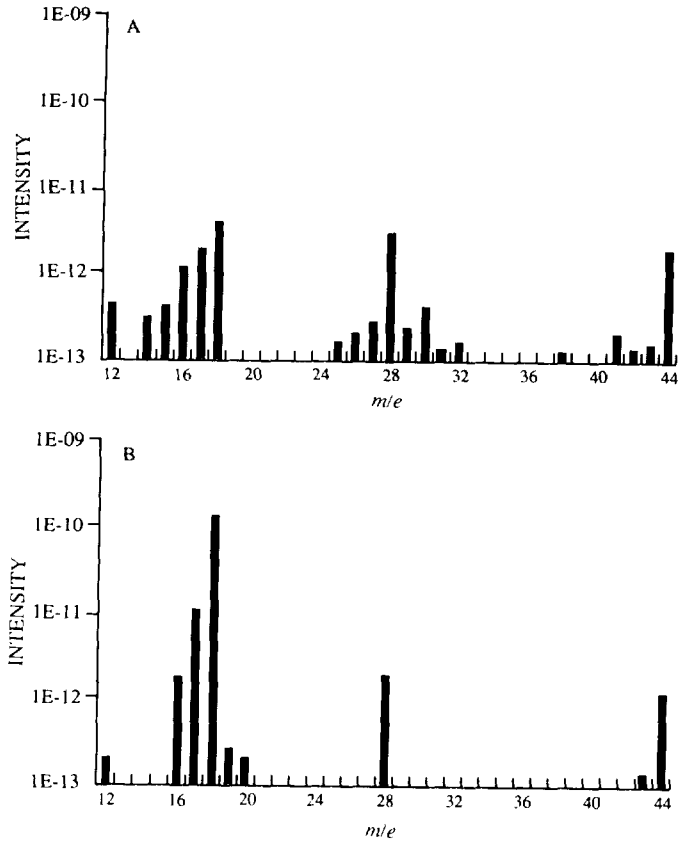

FIG. 10. Mass spectra of volatile products formed upon heating fluorohectorite clays at 250°C: (A) Li^+-fluorohectorite, (B) alumina-pillared fluorohectorite.

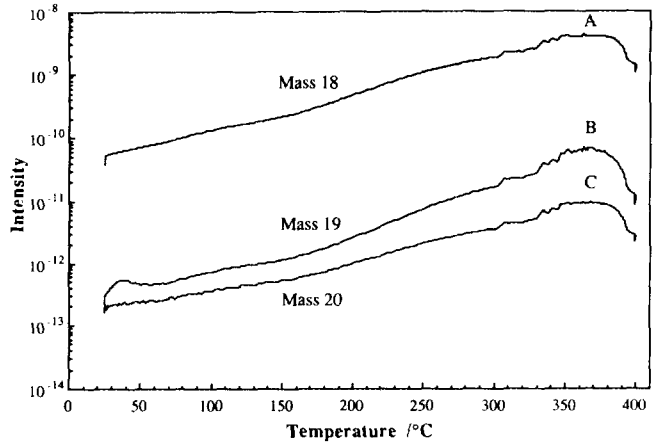

FIG. 11. Temperature dependence of the mass spectral intensities for the volatile products formed on heating alumina pillared fluorohectorite: (A) mass 18, (B) mass 19, and (C) mass 20.

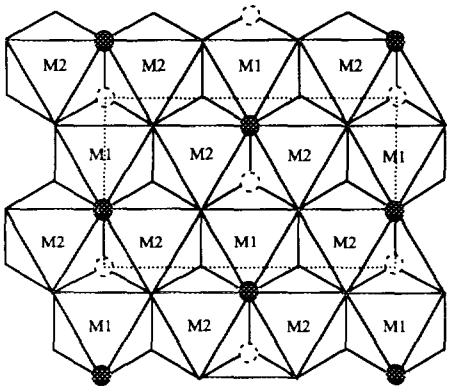

FIG. 12. Representation of the octahedral sheet in fluorohectorite (see text). Fluorine atoms are represented by full or dashed circles, depending whether they are above or below the layer plane. The dashed lines represent the octahedral sheet of an $O_{20}F_4$ unit cell.

Lewis and Brønsted acid mechanisms (cf. Fig. 3). On the other hand, alumina-pillared fluorohectorite calcined at 500°C (i.e., APF-500) is less active than a conventional alumina-pillared smectite clay such as montmorillonite. The differences in acidity appear to be related to the thermal behavior of fluorine in the 2 : 1 layered silicate framework. Thus, we consider first the significance of our ^{19}F MAS-NMR results.

Pristine Li^+-fluorohectorite exhibits two ^{19}F resonances at -10 and -16 ppm. The same two lines are found for Li^+-Laponite B, a related perfluorinated 2 : 1 structure with a lower charge density. Since the relative intensities of the ^{19}F resonances depend on layer charge density (cf. Fig. 6), the two fluorine environments are determined by the composition of the 2 : 1 silicate layers. In both clays all of the tetrahedral sites are occupied by silicon and all of the octahedral sites are occupied by Mg^{2+} and Li^+. However, the ratio of Mg^{2+} to Li^+ differs for the two clays.

In order to assign the fluorine resonance to specific layer environments, we consider the filling of the octahedral intersticies in a 2 : 1 layered structure. Figure 12 depicts the octahedral sheet of such a structure (*19*). Fluorine atoms are represented by full and open circles, depending on whether they are located in the upper or lower plane of the sheet. In a nonfluorinated clay these same positions would be occupied by hydroxyl groups. In an $O_{20}F_4$ framework unit cell, there are four fluorines and six octahedral intersticies. The fluorine atoms bridge three octahedral positions, which we refer to as "octahedral triads". Each octahedral triad consists of one M1-type octahedron in which the fluorine atoms are arranged at *trans* positions and two M2-type octahedra with the fluorines at *cis* positions. For a trioctahedral smectite in which all octahedral positions are filled by Mg^{2+} and Li^+ ions, the Li^+ ions will prefer to occupy M1-type octahedra in order to better distribute the net negative charge on the *trans* fluorines. The M2 sites filled by Mg^{2+} are formally electrically neutral. Thus, two types of octahedral triads are anticipated. One triad, designated T1, bears a net negative charge with

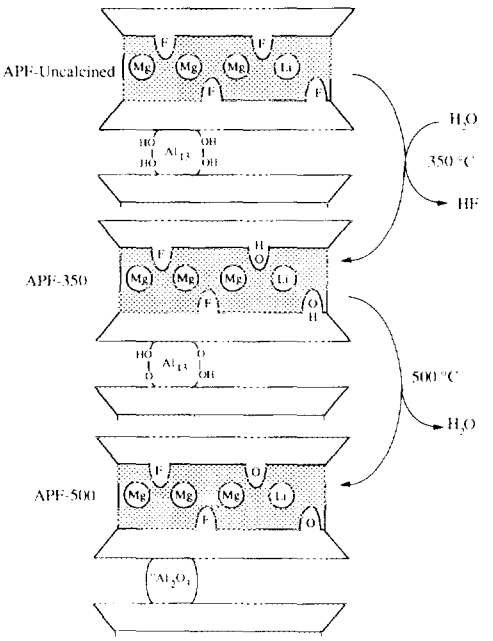

FIG. 13. Proposed model for the exchange of F by OH upon calcination of alumina-pillared fluorohectorite. The hexagonal holes in the tetrahedral sheet are represented by a dashed line.

Li^+ in a M1 site and two Mg^{2+} ions in M2 sites. The other triad, designated T2, is electrically neutral with the M1 and M2 octahedral sites filled by Mg^{2+}. Triads containing more than one Li^+ should be strongly disfavored on electrostatic grounds. The exceedingly weak resonance at -22 ppm in the spectrum of fluorohectorite (cf. Fig. 6A) might represent an Li_2Mg triad, though we cannot preclude the possibility of alternative assignments based on trace amounts of impurity phases.

For the two ^{19}F resonances in Li^+-fluorohectorite and Li^+-Laponite B, we assign the upfield line at -16 ppm to the fluorine atoms in electrically charged T1 triads. The downfield line at -10 ppm is attributed to the fluorines of neutral T2 triads. Analogous chemical shift assignments have been proposed recently by Huve *et al.* (*15*) in their ^{19}F NMR studies of a fluorinated hectorite. Our assignments are consistent with the more negatively charged fluorine occurring at higher field. For instance, the chemical shift for NaF and MgF_2 occur at -58 ppm and -31.8 ppm, respectively (*20*). Also, the shifts are in agreement with the layer charge densities of fluorohectorite and Laponite B. The layer unit cell formulas can be expressed in general as $[Mg_{6-x}Li_x]\,Si_8\,O_{20}F_4$, or, alternatively, as $[Mg_3]_{2-x}[Mg_2Li]_xO_{20}F_4$. The latter formulation indicates the T1 to T2 triad ratio to be $x/2-x$. Table 3 compares the octahedral metal ion compositions obtained by ^{19}F NMR with the compositions estimated from the cation-exchange capacities. The agreement in compositions confirms the chemical shift assignments. Included in the table are compositions obtained from chemical analyses. It would appear that the analytical results are less reliable estimates of composition, owing perhaps to the difficulty in achieving accurate analyses in the presence of fluorine.

We consider next the catalytic significance of the dramatic temperature dependence of the ^{19}F spectrum for the alumina-pillared derivative (cf. Fig. 7). As the pillared clay is heated in air to 350°C, a hydrolysis reaction occurs which preferentially replaces fluorine at charged T1 sites with hydroxyl groups. At 350°C, approximately 70% of the T1 fluorines have been hydrolyzed. Evidence for hydrolysis is provided by the concomitant appearance of an OH-stretching band at 3680 cm^{-1} characteristic of layer hydroxyl groups (cf. Fig. 8) (*16, 17, 21*). The preferential hydrolysis of fluorine in charged T1 sites presumably is the result of an energetically more favorable charge distribution within the layer framework.

Our mass spectroscopic results (cf. Figs. 10 and 11) indicate that HF can be detected as a volatile reaction product. It is unlikely that the replacement of fluorine by hydroxyls is accompanied by formation of SiF_4 or MgF_2, because these latter species should form with equal facility from fluorine in both T1 and T2 sites. Also, we find no experimental evidence for SiF_4 or MgF_2 by-products. Thus, the main mechanism for replacement of T1 fluorine by hydroxyls up to a reaction temperature of 350°C is the simple hydrolysis reaction. Further confirmation for hydrolysis is provided by the parallel relationship between the amount of water liberated in the hydrolysis process and the intensities of the mass 19 and 20 peaks characteristic of F^+ and HF^+ (cf. Fig. 11). Presumably, the water is supplied in large part by the dehydroxylation of the alumina pillars on the gallery surfaces.

A plausible pathway for the hydrolysis of T1 fluorines is the interlayer transport of water to the basal hexagonal cavities of the tetrahedral sheet, below which the fluorine atoms are located. The proposed mechanism is schematically illustrated in Fig. 13. It is important to emphasize that access to the hexagonal cavities is facilitated by the pillared galleries ($d_{(001)} \approx 18$ Å). No hydrolysis occurs for the collapsed Li^+-exchanged form of fluorohectorite ($d_{(001)} \approx 10$ Å at 350°C), as judged from the absence of layer OH vibrations in the FTIR spectrum (cf. Fig. 8).

The hydrolysis of the charged T1 fluorine sites in APF-350 most likely contributes significantly to the exceptional acidity of this pillared clay. It has been previously proposed that the calcination of non-fluorinated alumina-pillared clays, such as beidellite or montmorillonite, transforms the Al_{13} aggregates into a γ-Al_2O_3-type structure and causes protons to migrate to basic hydroxyl sites in the layers (*14*). These protons are liable and can migrate back to the gallery region for catalytic reaction. The layer hydroxyl groups of APF-350 can also act as binding sites for protons. Hydrolysis of the *trans* fluorine positions in T1 octahedral triads places the resulting hydroxyl groups at positions *cis* to the fluorines of adjacent neutral T2 triads (cf. Fig. 12). The electron-withdrawing effect of the *cis* fluorine will enhance the acidity of the protonated hydroxyl group, relative to a nonfluorinated smectite clay (cf. Fig. 13). That is, the dissociative equilibrium constant defined by the equation below is larger when the *cis* position X is fluorine rather than hydroxide:

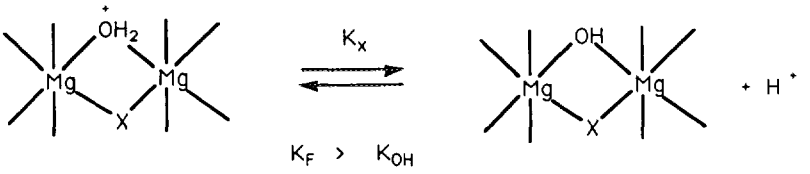

Although APF-350 is an exceptionally acidic pillared clay catalyst, a dramatic decrease in activity occurs when the clay is calcined at 500°C. The loss in acidity may be judged from the decrease in biphenyl alkylation activity (cf. Table 2), a 50% loss in ammonia binding capacity (cf. Fig. 1), and an order-of-magnitude decrease in pyridine chemisorption by Lewis and Brønsted acid mechanisms (cf. Fig. 3).

Several factors can contribute to the temperature sensitivity of an alumina-pillared clay catalyst. For instance, a decrease in the activity of an alumina-pillared montmorillonite catalyst has been observed for the gas phase conversion of 1, 2, 4-trimethylbenzene when the catalyst is calcined at 500°C. In this case the loss in activity most likely was due to loss of Brønsted acidity (*22*). However, for the liquid-phase alkylation of biphenyl, the reactivity of an alumina pillared clay is generally not sensitive to calcination temperature over the range 350–500°C. Thus, the difference in alkylation activity for APF-350 and APF-500 is atypical. Our previous studies of liquid-phase biphenyl alkylation suggest that reactivity depends in part on the meso- to micropore ratio. The pore structure is important for this reaction because the reaction is under diffusion control. However, the dramatic difference in acid catalytic activity between APF-350 and APF-500 cannot be traced to a substantial difference in pore structure. Both materials possess pillared microporous structures, as judged from the basal spacings and nitrogen surface area data (cf. Table 1).

The most likely cause of the reduced acidity for APF-500 is the dehydroxylation of the layers and associated structural rearrangements of the 2 : 1 layered structure. As shown by the FTIR spectra in Fig. 8, the intensity of the framework OH band at 3680 cm^{-1} decreases substantially upon calcining the clay at 500°C. If the structural hydroxyl groups are indeed the main source of catalytic activity in APF-350, then dehydroxylation explains why the activity is so repressed after calcination at 500°C. The rather substantial changes in the NMR chemical shifts for the tetrahedral ^{27}Al (cf. Fig. 4) and the ^{29}Si (cf. Fig. 5) resonances point to significant structural rearrangement of the pillars

and the layers. It has been previously suggested that the upfield chemical shift for the ^{29}Si resonance upon calcination is the result of crosslinking between the pillar and the layers (*11*). Structural changes upon calcination at 500°C also are indicated by the loss of an IR band at ~756 cm^{-1} for the pillar and the appearance of two new bands at 801 and 863 cm^{-1} (cf. Fig. 4). Although there is the possibility of the pillars reacting with liberated HF between 350 and 500°C, we find no evidence from ^{19}F MAS-NMR spectra for AlF_3 formation.

ACKNOWLEDGMENTS

J.-R. B. gratefully acknowledge a graduate fellowship from Rhône-Poulenc. Liam Moran is gratefully acknowledged for his help in setting up the ^{19}F MAS-NMR experiments. The authors also thank Gilles Gerard for his expertise in constructing the special IR cell used in this work. This research was supported in part by the National Science Foundation through Grant DMR-8903579.

REFERENCES

1. Getty, E. E., and Drago, R. S., *Inorg. Chem.* **29,** 1186 (1990).
2. Ghosh, A. K., and Kydd, R. A., *Catal. Rev.-Sci. Eng.* **27,** 539 (1985).
3. Hattori, H., Takahashi, O., Takagi, M., and Tanabe, K., *J. Catal.* **68,** 132 (1981).
4. Fijal, J., Zyla, M., and Tokarz, M., *Clay Miner.* **20,** 81 (1985).
5. Barrer, R. M., and Jones, D. L., *J. Chem. Soc. A* 1531 (1970).
6. Suzuki, E., Idemura, S., and Ono, Y., *Appl. Clay Sci.* **3,** 27 (1988).
7. Sakurai, H., Urabe, K., and Izumi, Y., *Bull. Chem. Soc. Jpn.* **62,** 3221 (1989).
8. Butruille, J.-R., and Pinnavaia, T. J., *Catal. Today* **14,** 141 (1992).
9. Schultz, A., Stone, W. E. E., Poncelet, G., and Fripiat, J. J., *Clays Clay Miner.* **35,** 251 (1987).
10. Busenberg, E., and Clemency, C. V., *Clays Clay Miner.* **21,** 213 (1973).
11. Pinnavaia, T. J., Landau, S. D., Tzou, M.-S., Johnson, I. D., and Lipsicas, M., *J. Am. Chem. Soc.* **107,** 7222 (1985).
12. Datka, J., *J. Chem. Soc. Faraday Trans. 1* **77,** 2877 (1981).
13. Fu, G., Nazar, L. F., and Bain, A. D., *Chem. Mater.* **3,** 602 (1991).
14. Tennakoon, D. T. B., Jones W., and Thomas, J. M., *J. Chem. Soc. Faraday Trans. 1* **82,** 3081 (1986).
15. Huve, L., Delmotte, L., Martin, P., LeDred, R., Baron, J. and Saehr, T., *Clays Clay Miner.* **40,** 186 (1992).
16. Poinsignon, C., Cases, J. M., and Fripiat, J. J., *J. Phys. Chem.* **82,** 1855 (1978).
17. Van Olphen, H., and Fripiat, J. J., "Data Handbook for Clay Minerals and other Non-Metallic Materials." Pergamon Press, London, 1979.
18. Nyquist, R., and Kagel, R., "Infrared Spectra of Inorganic Compounds (3800–45 cm^{-1})." Academic Press, New York, 1971.
19. Güven, N., *Rev. Mineral.* **19,** 493 (1989).
20. Kreinbrink, A. T., Sazavsky, C. D., Pyrz, J. W., Nelson, D. G. A., and Honkonen, R. S., *J. Magn. Reson.* **88,** 267 (1990).
21. Prost, R., "Etude de l'Hydratation des Argiles: Interaction Eau-Minéral et Mécanisme de la Rétention d'Eau." Thèse de Doctorate ès Sciences, Université Paris VI, 1975.
22. Matsuda, T., Asanuma, M., and Kikuchi, E., *Appl. Catal.* **38,** 289 (1988).